

Designing a Silymarin Nanopercolating System Using CME@ZIF-8: An Approach to Hepatic Injuries

Hui Yu,[○] Muhammad Saqib Saif,[○] Murtaza Hasan,^{*} Ayesha Zafar, Xi Zhao, Muhammad Waqas, Tuba Tariq, Huang Xue,^{*} and Riaz Hussain^{*}



Cite This: *ACS Omega* 2023, 8, 48535–48548



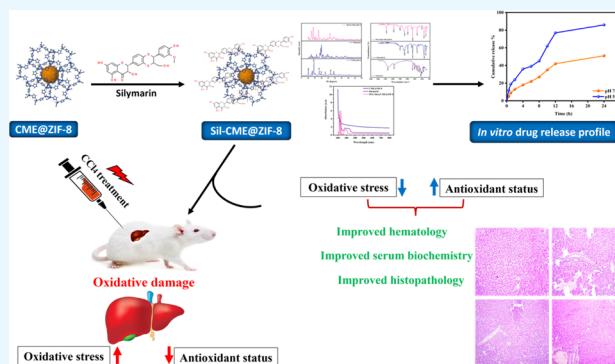
Read Online

ACCESS |

Metrics & More

Article Recommendations

ABSTRACT: It is commonly known that silymarin, a phytoconstituent obtained from the *Silybum marianum* plant, has hepatoprotective and antioxidative properties. However, its low oral bioavailability and poor water solubility negatively impact its therapeutic efficacy. The goal of the present study was to determine the efficiency of the *Cordia myxa* extract-based synthesized zeolitic imidazole metal–organic framework (CME@ZIF-8 MOF) for increasing silymarin's bioavailability. A coprecipitation technique was used to synthesize the CME@ZIF-8 and polyethylene glycol-coated silymarin-loaded MOFs (PEG-Sily@CME@ZIF-8) and a complete factorial design was used to optimize them. The crystalline size of CME@ZIF-8 was 14.7 nm and the size of PEG-Sily@CME@ZIF-8 was 17.39 nm. The loading percentage of the silymarin drug in CME@ZIF-8 was 33.5%. The optimized formulations were then characterized by ultraviolet–visible (UV–vis) spectroscopy, X-ray diffraction, Fourier transform IR spectroscopy, surface morphology, gas chromatography–mass spectrometry, and drug release in an in vitro medium. Additionally, a rat model was used to investigate the optimized formulation's in vivo hepatoprotective effectiveness. The synthesized silymarin-loaded CME@ZIF-8 MOFs were distinct particles with a porous, spongelike shape and a diameter of (size) nm. Furthermore, the designed silymarin-loaded PEG-Sily@CME@ZIF-8 MOF formulation exhibited considerable silymarin release from the synthesized formula in dissolution investigations. The in vivo evaluation studies demonstrated that the prepared PEG-Sily@CME@ZIF-8 MOFs effectively exhibited a hepatoprotective effect in comparison with free silymarin in a CCl₄-based induced-hepatotoxicity rat model via ameliorating the normal antioxidant enzyme levels and restoring the cellular abnormalities produced by CCl₄ toxication. In combination, biologically produced CME@ZIF-8 may promise to be a viable biologically based nanocarrier that can enhance the loading and release of silymarin medication, which has low solubility in water.



1. INTRODUCTION

Herbal medicines, also referred to as phytopharmaceuticals, have historically been utilized extensively in many nations to manage and cure a variety of medical conditions.¹ Due to their accessibility and a wide range of therapeutic uses, herbal medicine has become increasingly popular in modern medicine on a global scale.² However, plant extracts and phytoconstituents typically have poor in vivo efficiency because of their high molecular sizes and/or limited lipid solubility, which make them poorly absorbable and have less bioavailability.^{3,4}

The milk thistle (*Silybum marianum* (L.) Gaertn) seed contains a combination of flavonolignans known as silymarin (SIL). The primary active substance in this extract is silibinin, which is made up of silybin A and silybin B in a 50:50 ratio, along with silydianin, isosilycristin, isosilybin A, isosilybin B, silycristin, and taxifolin.⁵ SIL is a crucial hepatoprotective element used in clinics due to its diverse properties for liver fibrosis as antioxidant and anti-inflammatory. The main

barriers to SIL utilization include its water-based solubility-related bioavailability (0.5 g/L), high metabolism in extended phase II, quick excretion in bile and urine, and ineffective intestinal resorption.^{6,7} There have been several attempts to solubilize SIL, but none of them have had any positive pharmacological outcomes.⁸ The novel nanotechnology technique may be crucial in improving the bioavailability^{9–11} and pharmacological effects of substances, particularly plant-based substances.¹²

Drugs with low water solubility can be administered using a variety of technologies, such as solid dispersion, a decrease of

Received: October 27, 2023
Revised: November 20, 2023
Accepted: November 22, 2023
Published: December 7, 2023



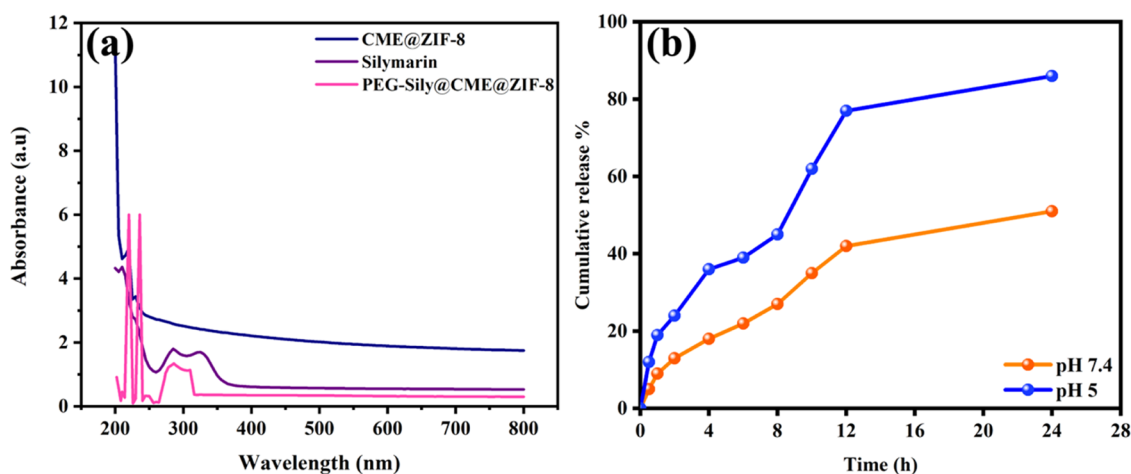


Figure 1. (a) UV absorbance spectrum of CME@ZIF-8, silymarin, and PEG-Sily@CME@ZIF-8; (b) drug release pattern from PEG-Sily@CME@ZIF-8 of ZIF-8 at different pH.

the drug crystalline size,¹³ the use of excipients (complexing agents, lipid formulations,¹⁴ surfactants, etc.) to increase solubility,¹⁵ and, more recently, utilizing nanoparticles as vehicles for the gradual and regulated release of pharmaceuticals,^{16,17} which also provides a way to solve the issues of availability and resistance while lowering the side effects.¹⁸ Targeted medication delivery using nanomaterials is crucial for diseases where the necessary dose cannot be given as usual, for example, because of poor blood flow to hard tissues.¹³ The potential for biomedical uses of drug-loaded nanomaterials is particularly intriguing. Among their advantages are the following: their nanometric size allows for easy modification/functionalization of their surface and control over their physicochemical properties.¹⁹ It also minimizes the potential for bioaccumulation in water media²⁰ and can reduce the toxicity of some drugs, allowing for optimal dosage.²¹ The ability to synthesize them with various morphologies to replicate the biological milieu in which they are delivered is another benefit.²²

There is considerable potential in porous materials like MOFs when used as nanocarriers for drugs. MOFs are a kind of polymers formed with the coordination of organic and metallic ligands that can form a decidedly porous structure with customized sizes and shapes.^{18,23} As a result of the use of different organic ligands and metal centers during their synthesis, plenty of MOFs are obtained having diverse physicochemical properties and crystalline forms.¹⁹

MIL-100, which was employed as a carrier to release ibuprofen, was the first framework used as a carrier for treatment.²² As a carrier of 5-fluorouracil,²⁰ doxorubicin,²⁴ and ibuprofen,²⁵ which are anti-inflammatory and anticancer drugs, new frameworks were produced recently, such as MIL-53¹⁸ and UiO-66.²⁶ Polydopamine²⁷ and poly(acrylic acid) (PAA)²⁸ are synthetic and natural polymers that have been used to modify the levels of MOFs and other carriers. In plenty of cases of drug delivery, this modification has revealed better outcomes.

An organometallic structure is formed by nitrogen atoms from the molecule of the organic ligand imidazole connected with the centered metal Zn^{2+} . This structure is known as zeolitic imidazolate framework-8 (ZIF-8 MOF).²⁹ It can carry molecules with high molecular weight, like therapeutic agents and drugs, due to its advantageous physicochemical character-

istics, i.e., volume and pore size. It remains more stable in neutral physiological media rather than in slightly acidic media because it is a pH-sensitive agent. It degrades at around 4.5–5 pH.³⁰ Due to this characteristic, it is capable of specific and localized release of the therapeutic agent. So, it is used to release medicine for diseases connected with cell acidification. In the present research, because of these features, ZIF-8 was chosen as the carrier of silymarin. As silymarin is poorly soluble in water and has low bioavailability, its nanoencapsulation strategy enhanced its solubility, absorption, and bioavailability and encouraged a longer drug release.³¹ Its encapsulated nanosized structure can pass membrane barriers easily, from which poorly soluble silymarin cannot pass, which could improve the weakly water-soluble silymarin's bioavailability and absorption.³² A higher absorption rate also means that a lower dosage of active ingredients (silymarin) is needed to provide the desired therapeutic effect.^{32,33}

The current study sought to increase silymarin's bioavailability and absorption by the formulation of the drug in a ZIF-8 nanocarrier system. To create and enhance the silymarin-loaded CME@ZIF-8, a coprecipitation approach was used. In the nanosize range, the synthesized structure revealed porous, virtually smooth layered surface particles. Additionally, competing with free silymarin, the synthesized formulation demonstrated a notable increase in the solubility of the loaded silymarin drug in an aqueous medium. Most significantly, in comparison with free silymarin, the optimized PEG-Sily@CME@ZIF-8 MOFs effectively enhanced the bioavailability of the silymarin and demonstrated a higher hepato-ameliorative effect in a CCl₄-treated liver toxicity rat model.

2. RESULTS AND DISCUSSION

2.1. Physicochemical Characterizations. We verified silymarin loading with CME@ZIF-8 with the help of ultraviolet–visible (UV–vis) spectra and compared the silymarin spectra with CME@ZIF-8 and PEG-Sily@CME@ZIF-8 spectra (Figure 1a). CME@ZIF-8 showed two peaks at 220 and 229 nm. Silymarin spectra also showed two peaks, one at 285 nm and the other at 326 nm, which matched with previous research,³⁴ while PEG-Sily@CME@ZIF-8 spectra had three peaks at 219, 235, and 285 nm; the peak at 285 nm of the PEG-Sily@CME@ZIF-8 spectra confirmed the presence of the silymarin drug in the MOF structure, while the band

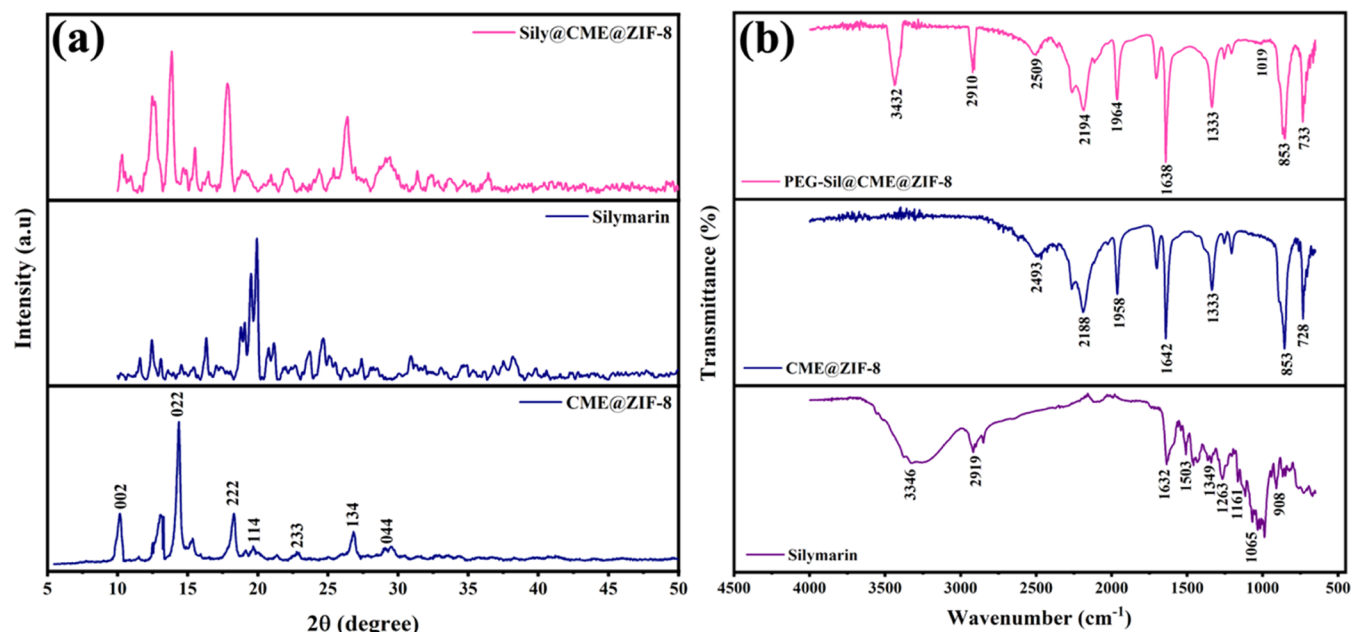


Figure 2. (a) XRD and (b) FTIR pattern of CME@ZIF-8, silymarin, and PEG-Sily@CME@ZIF-8.

Table 1. Crystal Size Calculation of CME@ZIF-8 Using the Scherrer Equation

peak no.	pos $2(\theta)$	intensity	fwhm left $2(\theta)$	b (rad)	size (nm)	average size (nm)
1	10.32614	24.23	0.36469	0.006365	21.87242155	17.39843155
2	12.55034	94.46	0.61287	0.010696	13.04057107	
3	13.80734	144.49	0.40085	0.006996	19.96334937	
4	15.48812	30.45	0.26835	0.004683	29.87668643	
5	17.81663	113.98	0.46614	0.008135	17.25079981	
6	26.33577	72.05	0.63679	0.011114	12.81240396	
7	29.20941	25.19	1.17737	0.020548	6.972788693	

Table 2. Crystal Size Calculation of PEG-Sily@CME@ZIF-8 Using the Scherrer Equation

	pos $2(\theta)$	intensity	fwhm left $2(\theta)$	b (rad)	size (nm)	average size (nm)
1	10.12371	1310.69	0.36857	0.006432	21.69702604	14.70510375
2	12.99167	1277.58	0.54942	0.009589	14.55283797	
3	14.3358	3008.48	0.36078	0.006296	22.19320514	
4	18.23921	1321.73	0.43041	0.007512	18.69378809	
5	19.61617	539.04	1.26369	0.022055	6.379828987	
6	22.7812	472.83	0.56697	0.009895	14.29336101	
7	26.78043	892.19	0.53588	0.009352	15.23901971	
8	29.2839	528.01	1.78819	0.031209	4.591763035	

shifting from 220 to 219 nm and from 229 to 235 nm is due to composite formation. This work supports the previous reports and confirms the current validity of the data.^{35,36}

The Fourier transform-infrared (FTIR) spectra of the free drug silymarin, CME@ZIF-8, and PEG-Sily@CME@ZIF-8 MOFs are presented in Figure 2b. The pure silymarin FTIR spectrum showed characteristic bands at 3428 cm^{-1} (O–H, phenols/alcohols), 2910 cm^{-1} (C–H, alkyl), 1629 cm^{-1} (C=O stretching), 1452 cm^{-1} (aromatic C=C ring stretching), 1273 cm^{-1} (C–O stretching, polyols), and 973 cm^{-1} (C–H bending, alkenes).³⁷ For CME@ZIF-8 characteristics, peaks are at 2485 cm^{-1} (O–H, carboxylic acid), 2186 cm^{-1} (C=C, alkynes), 1968 cm^{-1} (X = C = Y, isocyanate/isothiocyanate), 1628 cm^{-1} (C=C, alkenes), 1341 cm^{-1} (S = O, sulfate/sulfonamide), 850 cm^{-1} (C–H, aromatic stretch out of plane bend), and 728 cm^{-1} (C–X, chloride) functional

groups. For PEG-Sily@CME@ZIF-8 all of the bands are same as for CME@ZIF-8, but the characteristic bands at 2908 cm^{-1} (C–H, alkanes) and 3428 cm^{-1} (N–H, amine/amides stretch) demonstrated the successful encapsulation of the conventional silymarin drug within CME@ZIF-8 MOFs, as previously reported.^{38–40}

X-ray diffraction (XRD) analysis demonstrated that the PEG-Sily@CME@ZIF-8 MOFs had high crystallinity. Due to the encapsulation of the silymarin drug in the ZIF-8 crystal's pores, CME@ZIF-8 revealed broad peaks. The CME@ZIF-8 and PEG-Sily@CME@ZIF-8 peaks matched well with ZIF-8 (JCPDS 00–062–1030) and the cubic unit cell confirms it: $\alpha = \beta = \gamma = 90^\circ$ and $a = b = c = 17.0116 \text{ \AA}$.⁴¹ The XRD analysis diffractogram of silymarin showed sharp and intense peaks at $2\theta = 12.46, 16.41, 20.09, 24.64, 27.32, 31.06,$ and 38.24° , demonstrating silymarin's crystalline nature. The characteristic

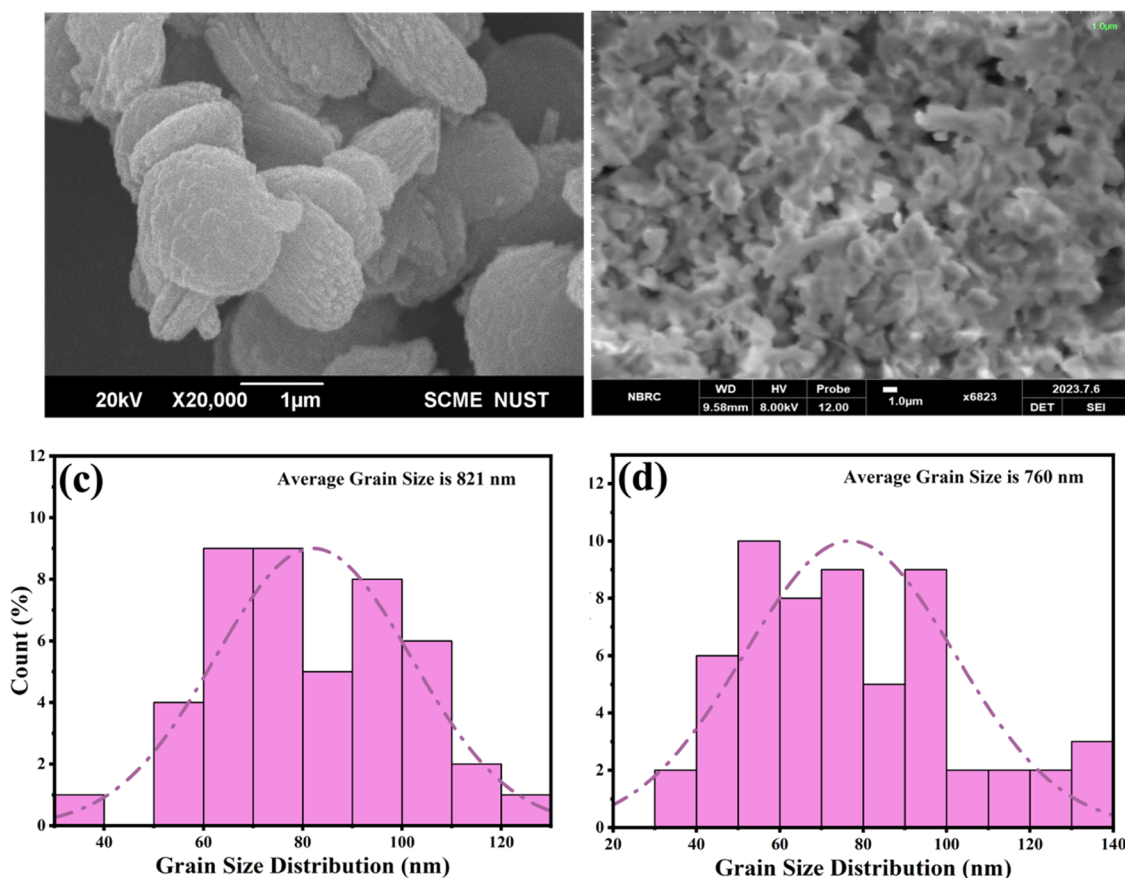


Figure 3. SEM of (a) CME@ZIF-8 and (b) PEG-Sily@CME@ZIF-8. Grain size distribution of (c) CME@ZIF-8 and (d) PEG-Sily@CME@ZIF-8.

Table 3. Molecular Weight, Properties, Formula, and Retention Time for Compounds Identified in Free Silymarin

no.	MF	compound name	mol. Wt (g/mol)	RT (m)	conc. %	properties
1	C ₃ H ₁₀ O ₂	hydroxymethyl cyclopropane	102.13	6.084	8.06	antioxidant, antifibrotic ⁵⁶
2	C ₆ H ₁₀ O ₅	1,6-Anhydro-β-d-talopyranose	162.41	12.624	7.93	antimicrobial ⁵⁷
3	C ₁₂ H ₂₂ O ₁₁	sucrose	342.30	14.687	27.41	antioxidant ⁵⁸
4	C ₆ H ₁₀ O ₅	levoglucosan	162.14	15.616	23.89	antioxidant, antimicrobial ⁵⁷
5	C ₁₂ H ₂₆ O ₃ si	methyl 3-((tert-butyl(dimethyl)silyl)oxy)-2-methylbutanoate	246.16	17.520	0.52	anti-inflammatory, anticancer ⁵⁹
6	C ₆ H ₁₀ O ₅	1,6-Anhydro-α-d-galactofuranose	161.14	18.194	6.87	antibacterial, antioxidant ⁶⁰
7	C ₁₀ H ₁₂ O ₃	4-((1E)-3-Hydroxy-1-propenyl)-2-methoxyphenol (coniferol)	180.2	21.348	1.19	antioxidant ⁶¹
8	C ₁₇ H ₃₄ O ₂	palmitic acid, methyl ester	270.5	24.962	12.20	antibacterial ⁶²
9	C ₁₆ H ₃₂ O ₂	n-hexadecenoic acid (palmitic acid)	256.42	25.808	1.96	antioxidant, anti-inflammatory ⁶³
10	C ₁₉ H ₃₄ O ₂	linoleic acid, methyl ester	295.5	28.210	1.45	antimicrobial, antioxidant ⁶⁴
11	C ₁₉ H ₃₆ O ₂	oleic acid, methyl ester	296.5	28.330	4.45	antimicrobial ⁶⁵
12	C ₁₇ H ₃₂ O ₂	methyl (7E)-7-hexadecenoate	268.24	28.460	1.60	antibacterial, antioxidant ⁶⁶
13	C ₁₈ H ₃₄ O ₂	oleic acid	282.5	29.237	1.18	antibacterial, antioxidant ⁶⁶
14	C ₁₈ H ₃₄ O ₂	octadecanoic acid (stearic acid)	282.5	29.734	1.30	antibacterial ⁶⁷

XRD peaks of CME@ZIF-8 at $2\theta = 10.05, 12.29, 14.46, 18.08, 22.72, 26.94,$ and 29.76° correspond to the planes of (002), (112), (022), (222), (044), (233), and (244), respectively.⁴²

The XRD analysis diffractogram of PEG-sily@CME@ZIF-8 at $2\theta = 10.05, 12.29, 14.46, 18.08, 22.72, 26.94,$ and 29.76° indicates the crystalline nature of ZIF-8, while the peaks at $17.81, 31.52,$ and 36.41° were due to the encapsulation of the silymarin drug in the ZIF-8 crystal's pores of CME@ZIF-8 (Figure 2a).

The crystalline size of the synthesized MOFs was determined by the Scherrer equation, given as⁴³

$$D = \frac{K\lambda}{\beta \cos \theta}$$

where D is the average crystal size of MOFs, K is the constant, λ is the X-ray wavelength, and θ is Bragg's angle, whereas β is the line broadening at full width at half-maximum (fwhm).⁴⁴ The average size of crystals of CME@ZIF-8 MOFs was 14.70 nm, Table 1, and the average size of PEG-Sily@CME@ZIF-8 was 17.39 nm, Table 2. The current work is supported by Garcia-Palacin et al.,⁴⁵ who synthesized ZIF-8 of size between 8 and 33 nm. The PEG-Sily@CME@ZIF-8 size is higher than that of CME@ZIF-8 MOFs, which is because of the

Table 4. Molecular Weight, Properties, Formula, and Retention Time for Compounds Identified in the CME@ZIF-8 MOFs

no.	MF	compound name	mol. Wt (g/mol)	RT (m)	conc. %	properties
1	C ₂₀ H ₃₈ O ₂	methyl 8-(2-octyl cyclopropyl) octanoate	310.5	21.722	3.74	antibacterial, antioxidant ⁷⁰
2	C ₁₇ H ₃₄ O ₂	hexadecanoic acid, methyl ester	270.5	23.817	36.83	antioxidant ⁷¹
3	C ₈ H ₁₆ O ₂	1,2-cyclohexanedimethanol	144.21	27.648	0.30	antioxidant, antiproliferative ⁷²
4	C ₁₆ H ₃₂ O ₂	1,E-11,Z-13-octadecatriene	256.42	27.879	0.28	anticancer ⁷³
5	C ₁₉ H ₃₄ O ₂	methyl (9E,12E)-9,12-octadecadienoate	294.5	28.210	3.57	antibacterial, antioxidant ⁷¹
6	C ₁₉ H ₃₆ O ₂	oleic acid, methyl ester	296.5	28.333	19.28	antimicrobial ⁶⁵
7	C ₁₇ H ₃₂ O ₂	7-hexadecenoic acid, methyl ester, (Z)-	268.4	28.459	6.76	antibacterial, antioxidant ⁶⁶
8	C ₁₉ H ₃₈ O ₂	stearic acid, methyl ester	298.5	28.842	27.77	antioxidant, antibacterial ⁷⁴
9	C ₁₅ H ₂₄	(1-methyl-1-propylpentyl) benzene	204.35	29.017	0.78	anti-inflammatory, antidiabetic ⁵⁹
10	C ₁₃ H ₂₀ O ₂	nopol acetate	208.30	29.266	0.98	antioxidant, analgesic, antipyretic ⁷⁵

Table 5. Molecular Weight, Properties, Formula, and Retention Time for Compounds Identified in PEG-Sily@CME@ZIF-8 MOFs

no.	MF	compound name	mol. Wt (g/mol)	RT (m)	conc. %	properties
1	C ₁₇ H ₃₄ O ₂	palmitic acid, methyl ester	270.5	24.968	38.15	antioxidant ⁷¹
2	C ₁₉ H ₃₄ O ₂	methyl(9E,12E)-9,12-octadecadienoate (linoleic acid)	294.5	28.216	3.95	antibacterial, antioxidant ⁶⁶
3	C ₁₉ H ₃₆ O ₂	oleic acid, methyl ester	296.5	28.336	17.77	antimicrobial ⁶⁵
4	C ₁₉ H ₃₆ O ₂	methyl(8E)-8-octadecenoate	296.5	28.467	7.02	antibacterial, antioxidant ⁷¹
5	C ₁₉ H ₃₈ O ₂	stearic acid, methyl ester (octadecenoic acid, methyl ester)	298.5	28.849	30.02	anticancer ⁷⁶
6	C ₁₅ H ₂₄	(1-methyl-1-propylpentyl) benzene	204.35	29.025	1.00	--
7	C ₂₁ H ₃₀ O ₂	3-phenyl propanoic acid, dodec-9-ynyl ester	314.5	29.277	1.15	antimicrobial
8	C ₁₈ H ₃₂ O ₂	cis-cis-linoleic acid	280.45	29.287	0.95	antimicrobial, antioxidant ⁶⁴

encapsulation of the silymarin drug in CME@ZIF-8 crystals, as mentioned in earlier reports.^{46–48}

The morphology of pure CME@ZIF-8 MOFs is like platelets with a layered surface as shown in scanning electron microscopy (SEM)⁴⁹ (Figure 3a) and, according to the SEM of PEG-Sily@CME@ZIF-8, revealed a sponge-shaped structure, which is different from that of CME@ZIF-8 crystals (Figure 3b). A comparison between these SEM images also confirmed the loading and encapsulation of the silymarin drug with CME@ZIF-8 MOFs. With the help of histogram analysis, the average grain size of PEG-Sily@CME@ZIF-8 and CME@ZIF-8 nanostructures was calculated using SEM.

In Figure 3c the average grain size of CME@ZIF-8 was determined to be 821 nm, while the average size of the grains of CME@ZIF-8 was measured as 760 nm (Figure 3d). These results matched with previous literature.⁵⁰

To identify the constituents responsible for the antioxidative action and to verify the loading of the silymarin drug into the CME@ZIF-8 structure, an inclusive analysis was performed, in which comparison between the retention times and concentration percentage of the compounds was performed with standard samples using GC-mass spectra from recognized databases like the PubChem (NIH), Wiley Libraries, Royal Society of Chemistry, and ChemSpider. This technique was employed to confirm the validated characterization and identification of the constituents and ensure the loading of silymarin drug within the CME@ZIF-8.

The identified compounds within CME@ZIF-8, silymarin, and PEG-Sily@CME@ZIF-8 with their molecular formula and molecular weight are listed in Tables 3, 4 and 5, respectively. The chromatograms of CME@ZIF-8, silymarin, and PEG-Sily@CME@ZIF-8 are shown in Figure 4. It was observed that palmitic acid, methyl ester, methyl(9E,12E)-9,12-octadecadienoate (linoleic acid), oleic acid, methyl ester, methyl(8E)-8-octadecenoate, stearic acid, methyl ester (octadecenoic acid, methyl ester), (1-methyl-1-propylpentyl) benzene, 3-phenyl

propanoic acid, dodec-9-ynyl ester, and cis-cis-linoleic acid are the compounds in the GC-MS of PEG-Sily@CME@ZIF-8 that were also found in the GC-MS analysis of CME@ZIF-8 as well as of silymarin, which confirmed the attachment of the silymarin drug into the CME@ZIF-8 MOF structure. The functional group and biofunctional compounds are very active and play a key role in the biological activities, as previously presented.^{51–55}

2.2. Nanoparticle Entrapment Efficiency (EE%). To determine the possible application of CME@ZIF-8 as the hepatoprotective system, the conventional antioxidative drug silymarin was loaded onto CME@ZIF-8 by a previously used drug loading method.⁶⁸ After 5 h, there was enough drug loading (33.05%); for poorly soluble drugs this is a significant percentage of the silymarin drug loading when related to previous literature.^{68,69} Hence, for the upcoming era of silymarin drug loading assays in the CME@ZIF-8 MOF system, 5 h of loading reaction is sufficient to reach the peak of loading capacity. According to our knowledge, in this study, a first-time plant extract with ZIF-8 MOF nanobiocomposite is being used for the incorporation of the silymarin drug. Therefore, this study confirms the significant capacity of ZIF-8 to encapsulate a large amount of silymarin.

2.3. In Vitro Drug Release Study. Silymarin was selected as a model drug to determine the possible application of CME@ZIF-8 MOFs as drug nanocarriers because CME@ZIF-8 is stable under physiological pH 7.4 and decomposes at acidic pH 5. It is important to highlight that although we have seen regulated delivery at various rates in both pHs, a quicker release has only been seen at pH 5. At pH 5, decomposition occurs by disassociation of the bonding between the ligands and the metal ions.²⁹ As a result, it is anticipated that at pH 7.4, the drug release will be significantly lower than at an acidic pH.⁷⁷ The drug release rates from PEG-Sily@CME@ZIF-8 are slower at pH 7.4 than they are at pH 5. As shown in Figure 1b, at pH 7.4, for the first 2 h, silymarin-loaded CME@ZIF-8

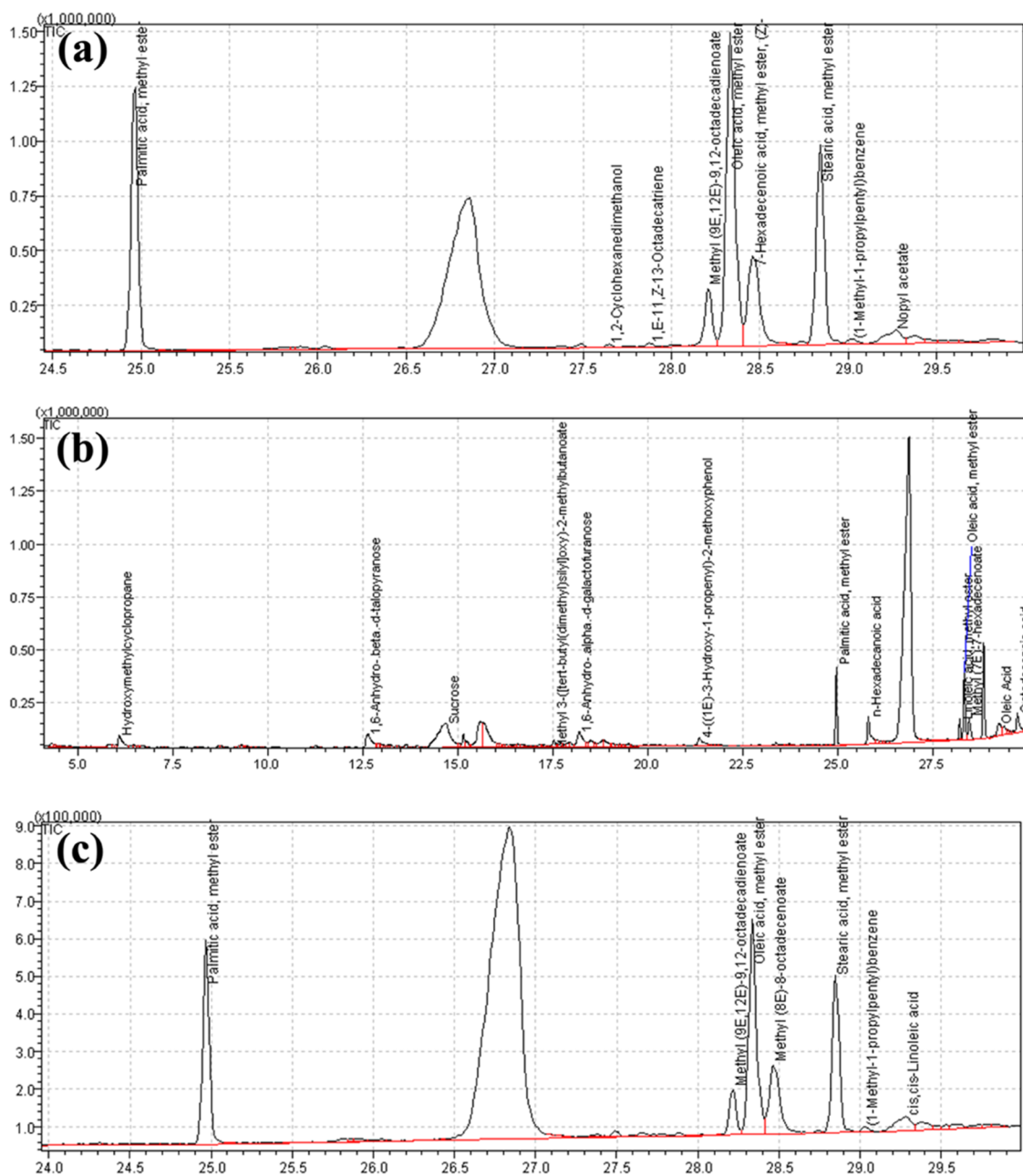


Figure 4. GC-MS chromatogram of (a) CME@ZIF-8, (b) silymarin, and (c) PEG-Sily@CME@ZIF-8.

represented a slow drug release of 13.21%, while for 12 h the drug-releasing rate was 41.25% and for 24 h it was 51.49%. At pH 5.0, the silymarin drug release profiles from CME@ZIF-8 exhibited a fast drug release at the starting; in the first 2 h of releasing it was 23.68%, followed by 76.96 and 85.79% at 12 and 24 h, respectively. In acidic conditions, the silymarin drug release from CME@ZIF-8 is significantly increased because of the destruction of CME@ZIF-8 in an acidic environment. Our research indicates that drug release can be regulated at physiological pH and that the drug can remain encapsulated within the CME@ZIF-8 framework. However, under acidic circumstances, drug release happens more quickly.

2.4. Toxicity of CME@ZIF-8 MOFs. The trial to check the toxicity of the synthesized CME@ZIF-8 MOFs spanned over 7 days, and in this period, in either the control or the MOF-treated groups, no death of rats was seen. The present work revealed that the intake of 1000 $\mu\text{g}/\text{kg}$ dose of CME@ZIF-8

and PEG-Sily@CME@ZIF-8 MOFs did not cause mortality in the model animals, indicating that this may be the highest dose that does not produce physical changes and is safe. There was no significant difference observed in the weight of control and MOF-treated albino rats throughout the study.

2.5. Hematological Parameters. In the present work, it has been seen that the rats treated with CME@ZIF-8 for 7 days did not show any effect on the blood parameters of the rats compared to the control group. However, after being treated with CCl_4 , the levels of different blood parameters such as mean corpuscular volume (MCV), white blood cells (WBC), and lymphocytes (LYM) increased, while other parameters such as red blood cells (RBC), hemoglobin (HGB), hematocrit (HCT), mean corpuscular hemoglobin (MCH), and hemoglobin concentration (MCHC) level decreased as compared to the control group. The increased and decreased levels of these parameters in the blood are,

Table 6. Hematological Profile of the Rats

treatment group	RBC ($10^6/\text{mm}^3$)	HGB (g/dl)	HCT (%)	MCV (fl)	MCH (pg)	MCHC (g/dl)	WBC ($10^3/\text{mm}^3$)	LYM (%)
I	7.16 ± 1.22	125 ± 1.65	41.03 ± 2.60	56.03 ± 4.07	17.90 ± 1.88	220.66 ± 8.36	3.53 ± 0.75	77.63 ± 8.70
II	3.89 ± 1.25	88 ± 30	23.45 ± 7.33	63.02 ± 2.83	21.17 ± 1.95	179.00 ± 5.16	6.82 ± 0.10	99.95 ± 1.5
III	7.49 ± 1.18	137 ± 4.89	42.12 ± 8.09	56.65 ± 1.36	18.30 ± 1.07	198.00 ± 1.41	4.94 ± 0.55	80.10 ± 2.55
IV	7.04 ± 1.46	113 ± 3.42	35.40 ± 0.83	53.50 ± 2.33	19.07 ± 0.75	223.75 ± 6.22	4.06 ± 1.08	85.07 ± 3.07
V	5.83 ± 1.34	109 ± 3.09	32.92 ± 0.46	60.57 ± 0.22	19.70 ± 0.51	194.75 ± 3.30	5.48 ± 1.25	89.50 ± 0.49
VI	6.58 ± 1.19	121 ± 5.56	41.40 ± 2.34	57.70 ± 0.49	18.22 ± 0.53	204.75 ± 2.21	4.54 ± 1.36	82.12 ± 1.00
VII	6.85 ± 1.11	131 ± 2.21	40.12 ± 1.12	54.55 ± 0.65	18.50 ± 0.62	230.75 ± 5.06	4.77 ± 1.48	82.17 ± 1.33

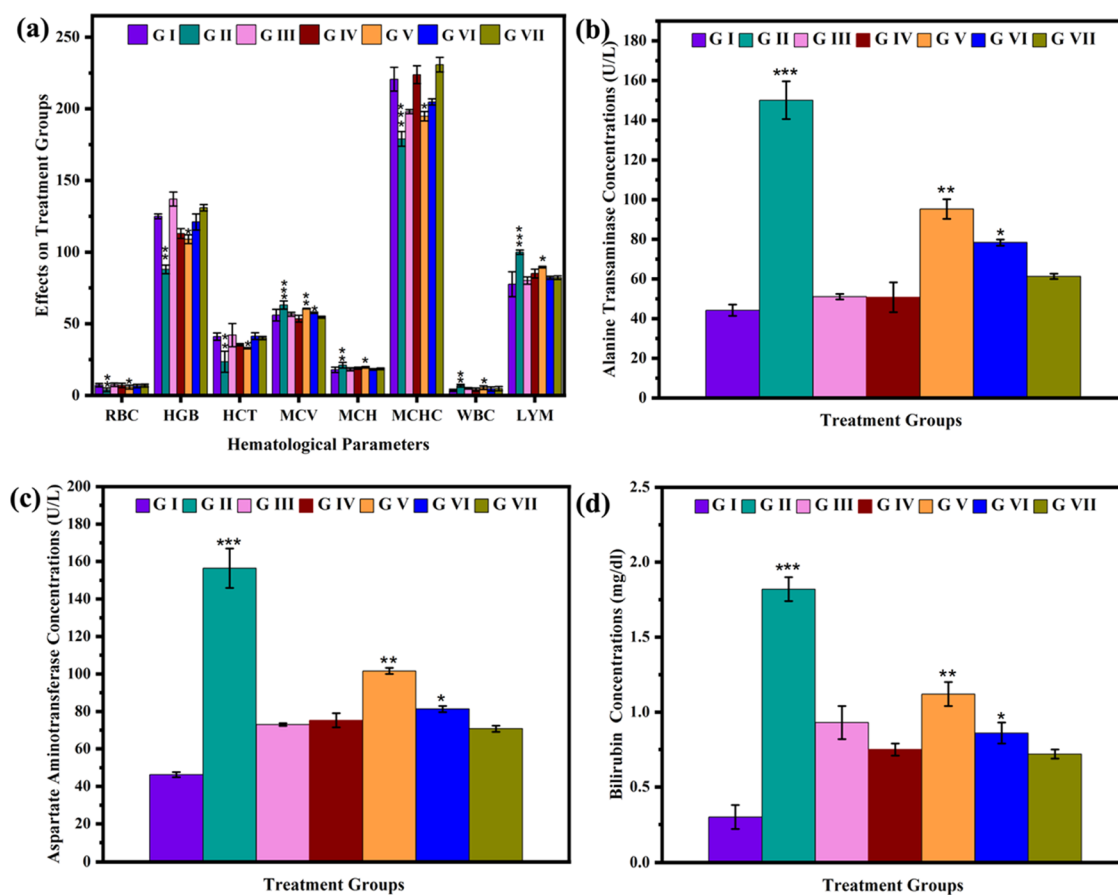


Figure 5. Comparison of various hematological parameters of the treated rats (a). Comparison of various serum parameters of the treated rats: alanine aminotransferase (b), aspartate aminotransferase (c), and bilirubin (d).

respectively, due to the oxidative stress and liver malfunctioning produced by CCl_4 . In group 3, after the 7 days of administration of silymarin in CCl_4 -treated rats, it was observed that WBC, MCV, and LYM levels in blood were decreased and RBC, HGB, HCT, MCH, and MCHC levels in blood increased; this is because of the protective behavior of the antioxidative drug silymarin. Groups 5, 6, and 7 were administered 500, 1000, and 1500 μg of silymarin-loaded MOFs of PEG-Sily@CME@ZIF-8, respectively, for 24 h, followed by the CCl_4 injection. It is observed that nanosilymarin decreases the CCl_4 infection rate and gradually decreases WBC, MCV, and LYM levels, and gradually increases RBC, HGB, HCT, MCH, and MCHC levels in the blood (Table 6). All of the silymarin-loaded drug-treated groups showed improved results, while the seventh group with 1500 μg showed the best results, in which the values of the blood parameters were near the control group. The pattern of hematology parameters' amelioration at different concentra-

tions of our synthesized nanosilymarin was 1500 $\mu\text{g}/\text{kg}$ bw >1000 $\mu\text{g}/\text{kg}$ bw >500 $\mu\text{g}/\text{kg}$ bw. It is revealed that PEG-Sily@CME@ZIF-8 gave significant results at a concentration very lower than that of the free silymarin drug (Figure 5a).

2.6. Analysis of the Serum Biochemistry. The levels of various liver biochemical biomarkers in the serum of all groups are listed in Table 7. The results indicated alanine aminotransferase (ALT), aspartate aminotransferase (AST), and bilirubin elevation after CCl_4 treatment when compared to the control group. In group 3, silymarin (100 mg/kg bw) treatment decreased the CCl_4 -induced elevation of serum biomarkers' ALT, AST, and albumin levels to levels similar to those of the control group. ALT, AST, and total bilirubin concentrations in serum did not differ significantly between rats treated with CME@ZIF-8 at 100 mg/kg bw alone (group 4) and control rats. The level of these biochemical markers was successfully restored to the control group by coadministering of PEG-Sily@CME@ZIF-8 (nanosilymarin) at low (500, 1000

Table 7. Serological Parameters of All of the Treated Groups

treatment group	ALT (μ /l)	AST (μ /l)	bilirubin (mg/dl)
I	44.23 \pm 2.85	46.22 \pm 1.32	0.30 \pm 0.13
II	150.08 \pm 9.52	156.44 \pm 10.52	1.82 \pm 0.08
III	51.10 \pm 1.38	72.99 \pm 0.77	0.93 \pm 0.11
IV	50.79 \pm 7.51	75.24 \pm 3.81	0.75 \pm 0.04
V	95.23 \pm 4.95	101.58 \pm 0.66	1.12 \pm 0.08
VI	78.34 \pm 1.53	81.26 \pm 0.64	0.86 \pm 0.33
VII	61.30 \pm 1.36	70.74 \pm 0.68	0.03

μ g/kg bw) and 1500 μ g/kg bw dosages. The level of hepatic biomarker restoration was in the order 1500 > 1000 > 500 μ g/kg bw (Figure b–d).

2.7. Microscopic Histopathological Examination. The image (Figure 6) depicts the histological alterations in coronal slices of the liver stained with hematoxylin and eosin. A microscopic examination of hepatic tissues of the control group of rats exhibited normal functions. Untreated rats had healthy liver structures, including lobule structure, portal hepatic space, and hepatocytes. Liver tissues treated with CCl₄ appeared fatty and pale yellow in color and microscopically exhibited severe histopathological disorders, including congestion, hemorrhages, pyknosis, nuclear hypertrophy, karyorrhexis, karyolysis, ceroid formation, and vacuolar degeneration (Table 8). However, the typical histological features of the liver tissues remained conserved with the administration of CME@ZIF-8 alone at 100 mg/kg bw, as in the control group. Following coadministration of a reference medicine, namely silymarin (group 3), the histological changes induced by CCl₄ were recovered, and the normal liver morphology with clear and distinct hepatocytes was apparent. Similarly, hepatopathological injuries were recovered by coadministration of PEG-Sily@ZIF-8 (nanosilymarin) at 500, 1000, and 1500 μ g/kg bw doses to CCl₄-intoxicated rats. The percentage of hepatocel-

Table 8. Level of Different Histopathological Lesions in Visceral Liver Tissues of Albino Rats

liver injuries	treatment groups						
	I	II	III	IV	V	VI	VII
congestion	-	++++	+++	+++	++++	+++	++
karyolysis	-	++++	++	++	+++	++	++
ceroid formation	-	+++	++	++	+++	++	++
karyorrhexis	-	++++	++	++	+++	++	++
vacuolar degeneration	-	++++	+++	+++	++++	+++	++
nuclear hypertrophy	-	++++	+++	+++	++++	+++	++
hemorrhages	-	+++	++	++	+++	++	++
pyknosis	-	++++	++	++	+++	++	++

lular injuries' amelioration at different dosages of nanosilymarin was in the order 1500 > 1000 > 500 μ g/kg bw. The current investigation is most related to work previously reported by the researchers.^{78,79}

2.8. Antioxidant Enzymes in the Liver. Table 9 provides an illustration of an investigation of the liver antioxidant enzyme status of treated rats. We observed tissue-specific damage in the CCl₄-treated rats (group two) along with a significant drop in the number of antioxidant enzymes such as catalase (CAT), superoxide dismutase (SOD), and peroxidase (POD). However, rats given silymarin as a conventional medication together with CCl₄ were protected from liver injury, as shown by a significantly higher level of these aforementioned markers. The concentration of these antioxidant markers was returned to control group values in CCl₄-treated rats by coadministration with PEG-Sily@ZIF-8 at 500, 1000, and 1500 μ g/kg bw dosages. The effect was more noticeable at a higher dosage of nanosilymarin (1500 μ g/kg) to CCl₄-induced rats, and the level of protection attained at this dose was comparable to that of silymarin plus CCl₄ treatment. However, administration of CME@ZIF-8 (100 mg/kg bw) alone to rats preserved the level of these marker

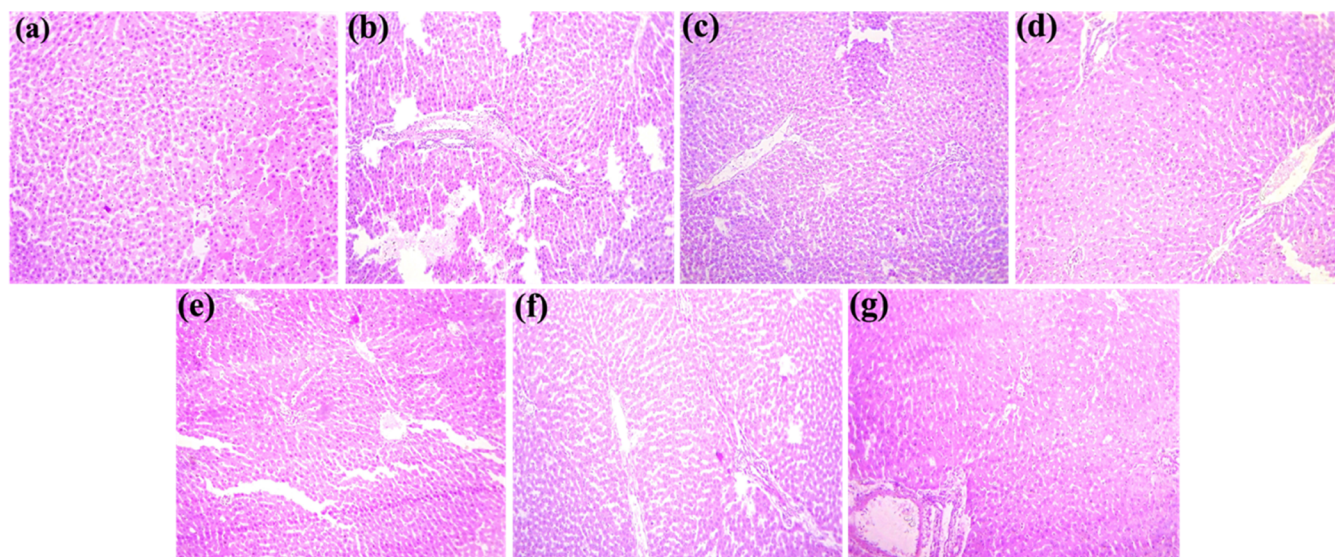


Figure 6. Histomicrograph showing different pathological changes in the liver of various treated groups of rats. (a) Normal histopathological pattern; (b) severe histopathological changes such as edema and inflammatory exudate; (c) moderate to severe histopathological changes such as pyknosis of hepatocytes; (d) mild to moderate histopathological changes such as degeneration of hepatocytes and atrophy of the nucleus of hepatocytes; (e) severe histopathological change on degeneration of hepatocytes and atrophy of the nucleus of hepatocytes; (f) moderate histopathological changes on nuclear and cytoplasmic degeneration; (g) moderate histopathological changes on nuclear and cytoplasmic degeneration.

Table 9. Antioxidative Enzymes and Oxidative Markers in Liver

treatment group	CAT (U/mg)	POD (U/mg)	SOD (U/mg)	TBARS (nM/mg protein)	ROS (OD)
I	6.07 ± 0.02	10.27 ± 0.24	5.43 ± 0.01	25.40 ± 0.15	0.46 ± 0.30
II	1.39 ± 0.38	2.04 ± 0.008	1.28 ± 0.01	49.31 ± 0.09	2.42 ± 0.16
III	4.78 ± 0.06	8.06 ± 0.003	4.31 ± 0.03	34.42 ± 0.08	0.96 ± 0.01
IV	6.47 ± 0.41	9.06 ± 0.01	5.30 ± 0.09	27.45 ± 0.21	0.44 ± 0.07
V	3.36 ± 0.39	6.09 ± 0.11	3.35 ± 0.03	41.53 ± 0.15	1.73 ± 0.18
VI	4.75 ± 0.19	8.04 ± 0.01	4.21 ± 0.02	34.24 ± 0.06	1.06 ± 0.08
VII	5.84 ± 0.17	9.05 ± 0.008	5.16 ± 0.06	26.33 ± 0.07	0.17

enzymes compared with control rats. It is observed that a low dose of PEG-Sily@ZIF-8 exhibited more efficient results in comparison to a high dose of the conventional drug silymarin. In this work, the elevation in antioxidant enzymes was observed in the following sequence: 1500 $\mu\text{g}/\text{kg}$ of bw > 1000 $\mu\text{g}/\text{kg}$ of bw > 500 $\mu\text{g}/\text{kg}$. This work is considered to be the most relevant and in confirmation with previous reports.^{80,81}

2.9. Biochemical Indices of the Liver. Table 9 shows that rats receiving CCl₄ had higher levels of biochemical indices of thiobarbituric acid reactive substances (TBARS) and reactive oxygen species (ROS) in their hepatic samples than those in the control group. Coadministration of free silymarin 100 mg/kg bw showed a significant restoration in these biochemical indices by dismissing the hepatotoxicity produced by CCl₄. On the other hand, coadministering PEG-Sily@CME@Zif-8 to CCl₄-treated rats at doses of 500, 1000, and 1500 $\mu\text{g}/\text{kg}$ bw gradually returned these parameters to those of control rats. PEG-Sily@CME@ZIF-8 1500 $\mu\text{g}/\text{kg}$ bw had restorative effects on liver parameters that were comparable to silymarin 100 mg/kg bw. It is observed that a low dose of PEG-Sily@CME@ZIF-8 exhibited more efficient results in comparison to the high dose of the conventional drug silymarin. Moreover, exposure to 100 mg/kg bw dose of CME@ZIF-8 alone did not have any effect on the tested biochemical markers in the treated groups.

3. EXPERIMENTAL SECTION

3.1. Materials. Zinc acetate hexahydrate, 2-methyl imidazole, polyethylene glycol 2000, dimethyl sulfoxide, carbon tetrachloride, and the other chemicals used for serology, oxidative and antioxidant enzymes, and histopathology were purchased from Sigma-Aldrich (USA). All chemicals and reagents used throughout the experiments were analytical grade or HPLC grade.

3.2. Synthesis of the PEG-Sily@CME@ZIF-8 Composite. For the preparation of PEG-Sily@CME@ZIF-8, the method was adopted from the previous literature with little modification.⁸² 1 g of CME@ZIF-8 was prepared as in our previous work,⁴⁹ soaked in silymarin solution (200 mg of silymarin in 40 mL of dimethyl sulfoxide (DMSO)). Then, the solution was covered and 24 h stirring was done, at room temperature. Sily-CME@ZIF-8 was synthesized with silymarin loaded within its structure and a yellowish color yield is obtained. To remove the adsorbed drug on the exterior surface, the loaded CME@ZIF-8 was cleaned thrice with methanol and deionized water (1:1 ratio) and centrifuged at 6000 rpm for 10 min. The supernatant was discarded, and the resulting yellow particles in the pallet were dried in an oven at 60 °C overnight. Further PEG was loaded to form the particles that were biocompatible for in vivo testing. The previously applied method was used with some modifications.⁸³ 250 mg of PEG-

Sily@CME@ZIF-8 was soaked in 25 mL of 1.6 mM PEG solution. After agitating for 24 h at room temperature, the mixture was washed using methanol and deionized water (1:1 ratio) 3 times with the help of a centrifuge machine at 6000 rpm for 10 min. The supernatant was discarded, and the obtained crystals were dried in a hot air oven for 24 h at 130 °C and stored for further characterization and applications. The drug loading percentage was determined using the following equation²⁹

$$\begin{aligned} &\text{drug loading percentage (\%)} \\ &= (\text{drug weight in sample} / \text{total weight of sample}) \\ &\quad \times 100\% \end{aligned}$$

3.3. Characterization. Different characterization techniques were used to confirm the formation of the desired MOFs. The absorption spectra patterns of CME@ZIF-8, silymarin, and PEG-Sily@CME@ZIF-8 MOFs were recorded between the range of 200–800 nm with a spectrophotometer (Agilent Cary 60 UV–vis). Infrared spectra were recorded to identify the different functional groups using the Agilent FTIR Spectrophotometer (Cary 360-ATR) with KBr pellets and a scanning range from 650 to 4000 cm^{-1} with a scanning speed of 32 cm^{-1} and a resolution of 4. For crystallinity determination, the XRD peaks of the samples were collected by Bruker D8 using a Cu K α source ($\lambda = 1.542 \text{ \AA}$) at 40 kV, 30 mA, and a scanning range of 5–80°. The chemical compounds in silymarin and PEG-Sily@CME@ZIF-8 were identified using gas chromatography–mass spectrometry analysis (GCMS-QP2010 Plus). To visualize the microscopic morphology of the products, scanning electron microscopy was performed using a scanning electron microscope (Cube 10, Emcraft South Korea).

3.4. In Vitro Drug Release Study. The typical systems for drug release studies were prepared by suspending 20 mg of PEG-Sily@CME@ZIF-8 in 50 mL of solutions (pH 5 and 7.4 buffers) with 0.1% Tween-20. Then, these suspensions were left at 37 °C and 250 rpm for 24 h in a shaker incubator. Aliquots of 2 mL were taken at different time spaces (0.5, 1, 2, 4, 6, 8, 12, and 24 h); each time, 2 mL of the sample was taken from both mediums (pH 7.4 and 5.0) and was replaced by the same volume of fresh buffer. The amount of the drug released from PEG-Sily@CME@ZIF-8 was noted by UV/vis spectroscopy at 288 nm.¹ The following formula was used to calculate the release percentage of the silymarin drug²⁹

$$\text{release percentage (\%)} = \text{mr} / \text{ml}$$

mr is the released amount of drug and ml is the total amount of encapsulated silymarin.

3.5. In Vivo Studies. **3.5.1. Animal Ethics.** Twenty-eight mature albino rats with weights between 250 and 300 g were purchased from the Department of Pharmacy, The Islamia

University of Bahawalpur, Pakistan. All of the animals were kept inside steel cages, each having four animals. The cages were kept in air-conditioned rooms with a 12 h light/dark cycle, 22–25 °C temperature, and 65 ± 4% relative humidity. The rodents were fed a normal rodent diet and given unlimited amounts of water during the study. The rats were put to prior acclimatization for 1 week before the experiment. The diet was withdrawn 12 h before the surgical procedure. The University's ethical committee gave its previous permission for all research and experiments, which were conducted in compliance with the National Institute of Health's "Guide for the Care and Use of Laboratory Animals" (NIH publication no. 85–23, 1985).

3.5.2. Dose Selection and Drug Administration. For studying the antioxidative (hepatoprotective) effects of the prepared nanosilymarin, all rats were divided into seven groups (having 4 rats each), and the dosing pattern was used according to the previously reported study.⁸²

Group I: Served as control and was fed only with normal food and clean water.

Group II: Animals in this group were intraperitoneally (ip) injected with CCl₄ in olive oil (1 mL/kg body weight; 3:7 v/v)

Group III: Animals in this group after 24 h of CCl₄ (30% v/v) treatment were intraperitoneally (i.p.) treated with the reference control drug silymarin (100 mg/kg body weight) for 7 days.

Group IV: Animals of this group were intraperitoneally (ip) injected with void CME@ZIF-8 nanoparticles for 7 days.

Group V: Animals of this group after 24 h of CCl₄ (30% v/v) were treated with nanosilymarin (PEG-Sily@CME@ZIF-8, 500 µg/kg body wt.) intraperitoneally (i.p.) for 7 days.

Group VI: Animals of this group after 24 h of CCl₄ (30% v/v) were treated with nanosilymarin (PEG-Sily@CME@ZIF-8, 1000 µg/kg body weight) intraperitoneally (ip) for 7 days.

Group VII: Animals of this group after 24 h of CCl₄ (30% v/v) were treated with nanosilymarin (PEG-Sily@CME@ZIF-8, 1500 µg/kg body wt.) intraperitoneally (i.p.) for 7 days.

After 7 days of trial completion, blood from each rat was obtained from the jugular vein in two types of tubes. Ethylenediaminetetraacetic acid (EDTA)-anticoagulated tubes were used to collect the blood for a biochemical examination. Blood was collected and centrifuged in tubes at 4000g for 15 min at 4 °C in a centrifuge machine in order to extract serum for analysis.⁸⁴ After dissection, immediately the liver was excised, washed with normal saline, weighed, and divided into two equal pieces; the one for biochemical and enzymatic assays was preserved at –80 °C, whereas the other was stored in 10% formalin solution for histopathological findings.⁸⁵

3.5.3. Physical Parameters. The feed intake was recorded daily. Different physical disorders like diarrhea, abnormal posture, anorexia, drowsiness, and behavioral changes were also examined daily. The body weight indexes were measured based on the initial body weight and final body weight using the formula final body weight–initial body weight/initial body weight × 100. The relative liver weight (% of body weight) was measured.⁸⁶

3.5.4. Hematology Parameters. The hematological profile of each rat from the treated and untreated groups was evaluated using an automated hematology analyzer. RBC counts, HGB, WBC counts, MCH, MCHC, MCV, PCV/(HCT), and lymphocytes were analyzed. The biomarkers for anemia are RBC, HGB, and HCT, which reflect the efficiency of hematopoietic tissues. MCV reflects the RBC size. On the

day of sampling, all hematological parameters were assessed within an hour after blood collection.

3.5.5. Serum Biochemistry Analysis. To evaluate hepatotoxicity, serum biochemical analysis was accomplished using standard laboratory techniques with a fully auto-chemistry analyzer (Beckmen Coulter-AU680). Thereafter, the levels of serum parameters ALT, AST, and total bilirubin in serum were determined to monitor the liver functions.

3.5.6. Histopathological Evaluation. For histopathology evaluation of liver, paraffin-fixed stained slices were used. Hematoxylin and eosin (H&E) stains were applied after a 4–5 µm thick segment of liver was sectioned from each group of rats using a microtome, dried, and embedded in paraffin wax. The slides were well examined by a highly experienced pathologist to analyze the protective aptitude of PEG-Sily@CME@ZIF-8 against CCl₄-intoxicated liver. A compound microscope (IRMECO IR-850) at 40× magnification was used for a thorough examination of the slides and photographed with a DSC-W810 camera.

3.5.7. Tissue Preparation and Biochemical Analyses. For the estimation of oxidative and antioxidant enzymes, the frozen livers were vigorously homogenized in 2 mL of PBS (100 mM, pH = 7.4) and left for 20 min at 4 °C before centrifugation. The homogenates were centrifuged at 6000 rpm for 5 min, and the supernatant was collected and preserved at 4 °C for further studies. Oxidative stress biomarkers in the livers such as ROS and TBARS were determined at 505 and 532 nm, respectively, while various antioxidant parameters such as CAT, SOD, and POD were determined at 240,⁸⁷ 560,⁸⁸ and 470 nm,⁸⁹ respectively, by a UV–vis spectrophotometer (752 UV). At least three readings were noted at intervals of 15 s.

3.5.8. Statistical Analysis. Using IBM SPSS for Windows version 8.1, the data from each experimental group were analyzed using the post hoc test and one-way analysis of variance (ANOVA). The collected data for the nanosilymarin-treated and control rat groups were presented as mean ± standard deviation for all measured CBC, serum biochemistry, and oxidative and antioxidant enzyme parameters. *P* ≤ 0.05 value was selected as a significant level.

4. CONCLUSIONS

This research work demonstrated the significance of CME@ZIF-8 MOFs for increasing the absorption, solubility, and in vivo hepatoprotective effects of silymarin. PEG-Sily@CME@ZIF-8 MOFs were fabricated using the coprecipitation method. In comparison to the plain medication, the optimized PEG-Sily@CME@ZIF-8 MOF formulation effectively increased the solubility of silymarin and maintained in vitro drug release for up to 24 h. Furthermore, the optimized PEG-Sily@CME@ZIF-8 MOF creation demonstrated better hepatoprotective effects in a CCl₄-induced-hepatotoxicity rat model compared to the plain drug. This was demonstrated by the effective reconstruction of normal levels of antioxidant enzymes and the amelioration of all cellular alterations induced by CCl₄ intoxication. Ultimately, our findings highlight the effectiveness of CME@ZIF-8-based silymarin (nanosilymarin) in enhancing the pharmacological effects of the poorly soluble medication silymarin by increasing its solubility and bioavailability.

AUTHOR INFORMATION

Corresponding Authors

Murtaza Hasan – Faculty of Chemical and Biological Science, Department of Biotechnology, The Islamia University of

Bahawalpur, Bahawalpur 63100, Pakistan; School of Chemistry and Chemical Engineering, Zhongkai University of Agriculture and Engineering, Guangzhou 510225, P. R. China; orcid.org/0000-0001-7715-9173; Email: murtaza@zhku.edu.cn

Huang Xue – School of Chemistry and Chemical Engineering, Zhongkai University of Agriculture and Engineering, Guangzhou 510225, P. R. China; Email: huangxue@zhku.edu.cn

Riaz Hussain – Faculty of Veterinary and Animal Sciences, Department of Pathology, The Islamia University of Bahawalpur, Bahawalpur 63100, Pakistan; Email: dr.riaz.hussain@iub.edu.pk

Authors

Hui Yu – College of Science, Beihua University, Jilin 132013, P. R. China

Muhammad Saqib Saif – Faculty of Chemical and Biological Science, Department of Biochemistry, The Islamia University of Bahawalpur, Bahawalpur 63100, Pakistan

Ayesha Zafar – School of Engineering, Royal Melbourne Institute of Technology (RMIT) University, Melbourne 3001, Australia

Xi Zhao – Institute of Theoretical Chemistry, College of Chemistry, Jilin University, Changchun 130021, P. R. China

Muhammad Waqas – Faculty of Chemical and Biological Science, Department of Biotechnology, The Islamia University of Bahawalpur, Bahawalpur 63100, Pakistan

Tuba Tariq – Faculty of Chemical and Biological Science, Department of Biochemistry, The Islamia University of Bahawalpur, Bahawalpur 63100, Pakistan

Complete contact information is available at:

<https://pubs.acs.org/10.1021/acsomega.3c08494>

Author Contributions

[○]H.Y. and M.S. contributed equally to this work.

Notes

The authors declare no competing financial interest.

ACKNOWLEDGMENTS

The authors would like to acknowledge the Islamia University Bahawalpur, Pakistan, National Research Program for University (NRPU) for Higher Education Commission, Pakistan (Grant ID: 9458). The authors are also thankful to Zhongkai University of Agriculture and Engineering, Guangzhou, China (510225) and the Guangdong Provincial Department of Agriculture and Rural affairs Project, Grant/Award Number 2020KJ115, 2021KJ115.

REFERENCES

- (1) Shriram, R. G.; Moin, A.; Alotaibi, H. F.; Khafagy, E. S.; Al Saqr, A.; Abu Lila, A. S.; Charyulu, R. N. Phytosomes as a Plausible Nano-Delivery System for Enhanced Oral Bioavailability and Improved Hepatoprotective Activity of Silymarin. *Pharmaceuticals* **2022**, *15* (7), No. 790, DOI: [10.3390/ph15070790](https://doi.org/10.3390/ph15070790).
- (2) Ekor, M. The Growing Use of Herbal Medicines: Issues Relating to Adverse Reactions and Challenges in Monitoring Safety. *Front. Pharmacol.* **2014**, *4*, No. 177, DOI: [10.3389/fphar.2013.00177](https://doi.org/10.3389/fphar.2013.00177).
- (3) Lu, M.; Qiu, Q.; Luo, X.; Liu, X.; Sun, J.; Wang, C.; Lin, X.; Deng, Y.; Song, Y. Phyto-Phospholipid Complexes (Phytosomes): A Novel Strategy to Improve the Bioavailability of Active Constituents. *Asian J. Pharm. Sci.* **2019**, *265*–274, DOI: [10.1016/j.ajps.2018.05.011](https://doi.org/10.1016/j.ajps.2018.05.011).
- (4) Aqil, F.; Munagala, R.; Jeyabalan, J.; Vadhanam, M. V. Bioavailability of Phytochemicals and Its Enhancement by Drug

Delivery Systems. *Cancer Lett.* **2013**, *133*–141, DOI: [10.1016/j.canlet.2013.02.032](https://doi.org/10.1016/j.canlet.2013.02.032).

(5) Ferenci, P. Silymarin in the Treatment of Liver Diseases: What Is the Clinical Evidence? *Clin. Liver Dis.* **2016**, *8*–10, DOI: [10.1002/clud.522](https://doi.org/10.1002/clud.522).

(6) Javed, S.; Kohli, K.; Ali, A. Reassessing Bioavailability of Silymarin 16. *Altern Med Rev.* **2011**, *16*, *3*, 239–249.

(7) Theodosiou, E.; Purchartová, K.; Stamatis, H.; Kolisis, F.; Křen, V. Bioavailability of Silymarin Flavonolignans: Drug Formulations and Biotransformation. *Phytochem. Rev.* **2014**, *13*, 1–18.

(8) Woo, J. S.; Kim, T.-S.; Park, J.-H.; Chp, S.-C. Formulation and Biopharmaceutical Evaluation of Silymarin Using SMEDDS. *Arch. Pharmacol. Res.* **2007**, *30*, 82–89, DOI: [10.1007/bf02977782](https://doi.org/10.1007/bf02977782).

(9) Dang, H.; Meng, M. H. W.; Zhao, H.; Iqbal, J.; Dai, R.; Deng, Y.; Lv, F. Luteolin-Loaded Solid Lipid Nanoparticles Synthesis, Characterization, & Improvement of Bioavailability, Pharmacokinetics in Vitro and Vivo Studies. *J. Nanopart. Res.* **2014**, *16*, No. 2347, DOI: [10.1007/s11051-014-2347-9](https://doi.org/10.1007/s11051-014-2347-9).

(10) Hasan, M.; Iqbal, J.; Awan, U.; Xin, N.; Dang, H.; Waryani, B.; Saeed, Y.; Ullah, K.; Dai, R.; Deng, Y. LX Loaded Nanoliposomes Synthesis, Characterization and Cellular Uptake Studies in H2O2 Stressed SH-SY5Y Cells. *J. Nanosci. Nanotechnol.* **2014**, *4066*–4071, DOI: [10.1166/jnn.2014.8201](https://doi.org/10.1166/jnn.2014.8201).

(11) Hasan, M.; Zafar, A.; Yousaf, M.; Gulzar, H.; Mehmood, K.; Hassan, S. G.; Saeed, A.; Yousaf, A.; Mazher, A.; Rongji, D.; Mahmood, N. Synthesis of Loureirin B-Loaded Nanoliposomes for Pharmacokinetics in Rat Plasma. *ACS Omega* **2019**, *4*, 6914–6922, DOI: [10.1021/acsomega.9b00119](https://doi.org/10.1021/acsomega.9b00119).

(12) Alipour, M.; Bigdeli, M. r.; Aligholi, H.; Rasoulia, B.; Khaksarian, M. Sustained Release of Silibinin-Loaded Chitosan Nanoparticle Induced Apoptosis in Glioma Cells. *J. Biomed. Mater. Res., Part A* **2020**, *108* (3), 458–469, DOI: [10.1002/jbm.a.36827](https://doi.org/10.1002/jbm.a.36827).

(13) Reddy, M. N.; Cheralathan, K. K.; Sasikumar, S. In Vitro Bioactivity and Drug Release Kinetics Studies of Mesoporous Silica-Biopolymer Composites. *J. Porous Mater.* **2015**, *22* (6), 1465–1472, DOI: [10.1007/s10934-015-0027-5](https://doi.org/10.1007/s10934-015-0027-5).

(14) Cao, D.; Shu, X.; Zhu, D.; Liang, S.; Hasan, M.; Gong, S. Lipid-Coated ZnO Nanoparticles Synthesis, Characterization and Cytotoxicity Studies in Cancer Cell. *Nano Convergence* **2020**, *7*, No. 14, DOI: [10.1186/s40580-020-00224-9](https://doi.org/10.1186/s40580-020-00224-9).

(15) Ramos, V. C.; Reyes, C. B. G.; García, G. M.; Quesada, M. I. S.; Barrero, F. J. M. C.; Rábago, J. J. S.; Polo, M. S. ZIF-8 and Its Magnetic Functionalization as Vehicle for the Transport and Release of Ciprofloxacin. *Pharmaceutics* **2022**, *14* (11), No. 2546, DOI: [10.3390/pharmaceutics14112546](https://doi.org/10.3390/pharmaceutics14112546).

(16) Lv, F.; Hasan, M.; Dang, H.; Hassan, S. G.; Meng, W.; Deng, Y.; Dai, R. Optimized Luteolin Loaded Solid Lipid Nanoparticle under Stress Condition for Enhanced Bioavailability in Rat Plasma. *J. Nanosci. Nanotechnol.* **2016**, *16* (9), 9443–9449, DOI: [10.1166/jnn.2016.11908](https://doi.org/10.1166/jnn.2016.11908).

(17) Hasan, M.; Ullah, I.; Zulfiqar, H.; Naeem, K.; Iqbal, A.; Gul, H.; Ashfaq, M.; Mahmood, N. Biological Entities as Chemical Reactors for Synthesis of Nanomaterials: Progress, Challenges and Future Perspective. *Mater. Today Chem.* **2018**, *8*, 13–28, DOI: [10.1016/j.mtchem.2018.02.003](https://doi.org/10.1016/j.mtchem.2018.02.003).

(18) Horcajada, P.; Serre, C.; Maurin, G.; Ramsahye, N. A.; Balas, F.; Vallet-Regí, M.; Sebban, M.; Taulelle, F.; Férey, G. Flexible Porous Metal-Organic Frameworks for a Controlled Drug Delivery. *J. Am. Chem. Soc.* **2008**, *130* (21), 6774–6780.

(19) Eshfahanian, M.; Ghasemzadeh, M. A.; Razavian, S. M. H. Synthesis, Identification and Application of the Novel Metal-Organic Framework Fe3O4@PAA@ZIF-8 for the Drug Delivery of Ciprofloxacin and Investigation of Antibacterial Activity. *Artif. Cells, Nanomed., Biotechnol.* **2019**, *47* (1), 2024–2030.

(20) Tan, L. L.; Song, N.; Zhang, S. X. A.; Li, H.; Wang, B.; Yang, Y. W. Ca²⁺, PH and Thermo Triple-Responsive Mechanized Zr-Based MOFs for on-Command Drug Release in Bone Diseases. *J. Mater. Chem. B* **2016**, *4* (1), 135–140.

- (21) Ali, A.; Saeed, S.; Hussain, R.; Afzal, G.; Siddique, A. B.; Parveen, G.; Hasan, M.; Caprioli, G. Synthesis and Characterization of Silica, Silver-Silica, and Zinc Oxide-Silica Nanoparticles for Evaluation of Blood Biochemistry, Oxidative Stress, and Hepatotoxicity in Albino Rats. *ACS Omega* **2023**, *8* (23), 20900–20911, DOI: 10.1021/acsomega.3c01674.
- (22) Horcajada, P.; Serre, C.; Vallet-Regí, M.; Sebban, M.; Taulelle, F.; Férey, G. Metal-Organic Frameworks as Efficient Materials for Drug Delivery. *Angew. Chem., Int. Ed.* **2006**, *45* (36), 5974–5978.
- (23) Costa, B. A.; Abuçafy, M. P.; Barbosa, T. W. L.; da Silva, B. L.; Fulindi, R. B.; Isquibola, G.; da Costa, P. I.; Chiavacci, L. A. ZnO@ZIF-8 Nanoparticles as Nanocarrier of Ciprofloxacin for Antimicrobial Activity. *Pharmaceutics* **2023**, *15* (1), No. 259, DOI: 10.3390/pharmaceutics15010259.
- (24) Zheng, H.; Zhang, Y.; Liu, L.; Wan, W.; Guo, P.; Nyström, A. M.; Zou, X. One-Pot Synthesis of Metal-Organic Frameworks with Encapsulated Target Molecules and Their Applications for Controlled Drug Delivery. *J. Am. Chem. Soc.* **2016**, *138* (3), 962–968.
- (25) Motakef-Kazemi, N.; Shojaosadati, S. A.; Morsali, A. In Situ Synthesis of a Drug-Loaded MOF at Room Temperature. *Microporous Mesoporous Mater.* **2014**, *186*, 73–79.
- (26) Zhu, X.; Gu, J.; Wang, Y.; Li, B.; Li, Y.; Zhao, W.; Shi, J. Inherent Anchorages in UiO-66 Nanoparticles for Efficient Capture of Alendronate and Its Mediated Release. *Chem. Commun.* **2014**, *50* (63), 8779–8782.
- (27) Zhang, M.; Zhang, L.; Chen, Y.; Li, L.; Su, Z.; Wang, C. Precise Synthesis of Unique Polydopamine/Mesoporous Calcium Phosphate Hollow Janus Nanoparticles for Imaging-Guided Chemo-Photothermal Synergistic Therapy. *Chem. Sci.* **2017**, *8* (12), 8067–8077.
- (28) Zhang, L.; Chen, Y.; Li, Z.; Li, L.; Saint-Cricq, P.; Li, C.; Lin, J.; Wang, C.; Su, Z.; Zink, J. I. Tailored Synthesis of Octopus-type Janus Nanoparticles for Synergistic Actively-Targeted and Chemo-Photothermal Therapy. *Angew. Chem.* **2016**, *128* (6), 2158–2161.
- (29) Nabipour, H.; Sadr, M. H.; Bardajee, G. R. Synthesis and Characterization of Nanoscale Zeolitic Imidazolate Frameworks with Ciprofloxacin and Their Applications as Antimicrobial Agents. *New J. Chem.* **2017**, *41* (15), 7364–7370.
- (30) Kaur, H.; Mohanta, G. C.; Gupta, V.; Kukkar, D.; Tyagi, S. Synthesis and Characterization of ZIF-8 Nanoparticles for Controlled Release of 6-Mercaptopurine Drug. *J. Drug Delivery Sci. Technol.* **2017**, *41*, 106–112.
- (31) Telange, D. R.; Patil, A. T.; Pethe, A. M.; Fegade, H.; Anand, S.; Dave, V. S. Formulation and Characterization of an Apigenin-Phospholipid Phytosome (APLC) for Improved Solubility, in Vivo Bioavailability, and Antioxidant Potential. *Eur. J. Pharm. Sci.* **2017**, *108*, 36–49, DOI: 10.1016/j.ejps.2016.12.009.
- (32) Yang, K. Y.; Hwang, D. H.; Yousaf, A. M.; Kim, D. W.; Shin, Y. J.; Bae, O. N.; Kim, Y. Il.; Kim, J. O.; Yong, C. S.; Choi, H. G. Silymarin-Loaded Solid Nanoparticles Provide Excellent Hepatic Protection: Physicochemical Characterization and in Vivo Evaluation. *Int. J. Nanomed.* **2013**, *8*, 3333–3343, DOI: 10.2147/IJN.S50683.
- (33) Alharbi, W. S.; Almughem, F. A.; Almeahmady, A. M.; Jarallah, S. J.; Alsharif, W. K.; Alzahrani, N. M.; Alshehri, A. A. Phytosomes as an Emerging Nanotechnology Platform for the Topical Delivery of Bioactive Phytochemicals. *Pharmaceutics* **2021**, *13*, No. 1475, DOI: 10.3390/pharmaceutics13091475.
- (34) Svobodová, A. R.; Gabrielová, E.; Michaelides, L.; Kosina, P.; Ryšavá, A.; Ulrichová, J.; Zálesák, B.; Vostálová, J. UVA-Photoprotective Potential of Silymarin and Silybin. *Arch. Dermatol. Res.* **2018**, *310* (5), 413–424, DOI: 10.1007/s00403-018-1828-6.
- (35) Luo, F.; Zeng, D.; Chen, R.; Zafar, A.; Weng, L.; Wang, W.; Tian, Y.; Hasan, M.; Shu, X. PEGylated Dihydromyricetin-Loaded Nanoliposomes Coated with Tea Saponin Inhibit Bacterial Oxidative Respiration and Energy Metabolism. *Food Funct.* **2021**, *12* (19), 9007–9017, DOI: 10.1039/D1FO01943K.
- (36) Naz, G.; Shabbir, M.; Ramzan, M.; Haq, B. U.; Arshad, M.; Tahir, M. B.; Hasan, M.; Ahmed, R. Synergistic Effect of Cu/Mgx and Zn1-xO for Enhanced Photocatalytic Degradation and Antibacterial Activity. *Phys. B Condens. Matter* **2022**, *624*, No. 413396, DOI: 10.1016/j.physb.2021.413396.
- (37) Abdullah, A. S.; El Sayed, I. E. T.; El-Torgoman, A. M. A.; Alghamdi, N. A.; Ullah, S.; Wageh, S.; Kamel, M. A. Preparation and Characterization of Silymarin-Conjugated Gold Nanoparticles with Enhanced Anti-Fibrotic Therapeutic Effects against Hepatic Fibrosis in Rats: Role of Micrnas as Molecular Targets. *Biomedicines* **2021**, *9* (12), No. 1767, DOI: 10.3390/biomedicines9121767.
- (38) Nadeem, M. S.; Munawar, T.; Mukhtar, F.; Batool, S.; Hasan, M.; Akbar, U. A.; Hakeem, A. S.; Iqbal, F. Energy-Levels Well-Matched Direct Z-Scheme ZnNiNdO/CdS Heterojunction for Elimination of Diverse Pollutants from Wastewater and Microbial Disinfection. *Environ. Sci. Pollut. Res.* **2022**, *29*, 50317–50334, DOI: 10.1007/s11356-022-19271-2.
- (39) Munawar, T.; Mukhtar, F.; Nadeem, M. S.; Manzoor, S.; Ashiq, M. N.; Riaz, M.; Batool, S.; Hasan, M.; Iqbal, F. Facile Synthesis of Rare Earth Metal Dual-Doped Pr2O3 Nanostructures: Enhanced Electrochemical Water-Splitting and Antimicrobial Properties. *Ceram. Int.* **2022**, *48* (13), 19150–19165, DOI: 10.1016/j.ceramint.2022.03.206.
- (40) Hasan, M.; Zafar, A.; Jabbar, M.; Tariq, T.; Manzoor, Y.; Ahmed, M. M.; Hassan, S. G.; Shu, X.; Mahmood, N. Trident Nano-Indexing the Proteomics Table: Next-Version Clustering of Iron Carbide NPs and Protein Corona. *Molecules* **2022**, *27* (18), No. 5754, DOI: 10.3390/molecules27185754.
- (41) Schejn, A.; Balan, L.; Falk, V.; Aranda, L.; Medjahdi, G.; Schneider, R. Controlling ZIF-8 Nano- and Microcrystal Formation and Reactivity through Zinc Salt Variations. *CrystEngComm* **2014**, *16* (21), 4493–4500, DOI: 10.1039/C3CE42485E.
- (42) Nguyen, L. T. L.; Le, K. K. A.; Phan, N. T. S. A Zeolite Imidazolate Framework ZIF-8 Catalyst for Friedel-Crafts Acylation. *Chin. J. Catal.* **2012**, *33* (4), 688–696, DOI: 10.1016/S1872-2067(11)60368-9.
- (43) Saif, M. S.; Zafar, A.; Waqas, M.; Hassan, S. G.; Haq, A. ul.; Tariq, T.; Batool, S.; Dilshad, M.; Hasan, M.; Shu, X. Phyto-Reflexive Zinc Oxide Nano-Flowers Synthesis: An Advanced Photocatalytic Degradation and Infectious Therapy. *J. Mater. Res. Technol.* **2021**, *13*, 2375–2391.
- (44) Sasaki, K.; Okue, T.; Shu, Y.; Miyake, K.; Uchida, Y.; Nishiyama, N. Thin ZIF-8 Nanosheets Synthesized in Hydrophilic TRAPs. *Dalton Trans.* **2021**, 10394–10399, DOI: 10.1039/d1dt01507a.
- (45) García-Palacín, M.; Martínez, J. I.; Pasetta, L.; Deacon, A.; Johnson, T.; Malankowska, M.; Téllez, C.; Coronas, J. Sized-Controlled ZIF-8 Nanoparticle Synthesis from Recycled Mother Liquors: Environmental Impact Assessment. *ACS Sustainable Chem. Eng.* **2020**, *8* (7), 2973–2980.
- (46) Luo, F.; Zeng, D.; Wang, W.; Yang, Y.; Zafar, A.; Wu, Z.; Tian, Y.; Huang, Y.; Hasan, M.; Shu, X. Bio-Conditioning Poly-Dihydromyricetin Zinc Nanoparticles Synthesis for Advanced Catalytic Degradation and Microbial Inhibition. *J. Nanostruct. Chem.* **2022**, *12*, 903–917, DOI: 10.1007/s40097-021-00443-4.
- (47) Munawar, T.; Mukhtar, F.; Nadeem, M. S.; Manzoor, S.; Ashiq, M. N.; Mahmood, K.; Batool, S.; Hasan, M.; Iqbal, F. Fabrication of Dual Z-Scheme TiO2-WO3-CeO2 Heterostructured Nanocomposite with Enhanced Photocatalysis, Antibacterial, and Electrochemical Performance. *J. Alloys Compd.* **2022**, *898*, No. 162779, DOI: 10.1016/j.jallcom.2021.162779.
- (48) Hasan, M.; Gulzar, H.; Zafar, A.; ul Haq, A.; Mustafa, G.; Tariq, T.; Khalid, A.; Mahmood, A.; Shu, X.; Mahmood, N. Multiplexing Surface Anchored Functionalized Iron Carbide Nanoparticle: A Low Molecular Weight Proteome Responsive Nano-Tracer. *Colloids Surf., B* **2021**, *203*, No. 111746, DOI: 10.1016/j.colsurfb.2021.111746.
- (49) Saif, M. S.; Hasan, M.; Zafar, A.; Ahmed, M. M.; Tariq, T.; Waqas, M.; Hussain, R.; Zafar, A.; Xue, H.; Shu, X. Advancing Nanoscale Science: Synthesis and Bioprinting of Zeolitic Imidazole Framework-8 for Enhanced Anti-Infectious Therapeutic Efficacies. *Biomedicines* **2023**, *11* (10), No. 2832, DOI: 10.3390/biomedicines11102832.

- (50) Nordin, N. A. H. M.; Ismail, A. F.; Mustafa, A.; Murali, R. S.; Matsuura, T. The Impact of ZIF-8 Particle Size and Heat Treatment on CO₂/CH₄ Separation Using Asymmetric Mixed Matrix Membrane. *RSC Adv.* **2014**, *4* (94), 52530–52541.
- (51) Huang, X.; Zafar, A.; Ahmad, K.; Hasan, M.; Tariq, T.; Gong, S.; Hassan, S. G.; Guo, J.; Javed, H. U.; Shu, X. Biological Synthesis of Bimetallic Hybrid Nanocomposite: A Remarkable Photocatalyst, Adsorption/Desorption and Antimicrobial Agent. *Appl. Surf. Sci. Adv.* **2023**, *17*, No. 100446, DOI: 10.1016/j.apsadv.2023.100446.
- (52) Ran, Y.; Xu, B.; Wang, R.; Gao, Q.; Jia, Q.; Hasan, M.; Shan, S.; Ma, H.; Dai, R.; Deng, Y.; Qing, H. Dragon's Blood Extracts Reduce Radiation-Induced Peripheral Blood Injury and Protects Human Megakaryocyte Cells from GM-CSF Withdraw-Induced Apoptosis. *Phys. Med.* **2016**, *32* (1), 84–93, DOI: 10.1016/j.ejmp.2015.09.010.
- (53) Ran, Y.; Wang, R.; Lin, F.; Hasan, M.; Jia, Q.; Tang, B.; Xia, Y.; Shan, S.; Wang, X.; Li, Q.; Deng, Y.; Qing, H. Radioprotective Effects of Dragon's Blood and Its Extract against Gamma Irradiation in Mouse Bone Marrow Cells. *Phys. Med.* **2014**, *30* (4), 427–431, DOI: 10.1016/j.ejmp.2013.12.001.
- (54) Shaheen, S.; Hasan, M.; Dilshad, M.; Zafar, A.; Tariq, T.; Shaheen, A.; Iqbal, R.; Ali, Z.; Munawar, T.; Iqbal, F.; Hassan, S. G.; Shu, X.; Caprioli, G. Green Synthesized ZnO-Fe₂O₃-Co₃O₄ Nanocomposite for Antioxidant, Microbial Disinfection and Degradation of Pollutants from Wastewater. *Biochem. Syst. Ecol.* **2022**, *105*, No. 104535.
- (55) Cheng, X.; Zou, Q.; Zhang, H.; Zhu, J.; Hasan, M.; Dong, F.; Liu, X.; Li, J.; Wu, Y.; Lv, X.; Wang, K.; Deng, X.; Liu, Z.; Jiang, X. Effects of a Chitosan Nanoparticles Encapsulation on the Properties of Litchi Polyphenols. *Food Sci. Biotechnol.* **2023**, *32*, 1861–1871, DOI: 10.1007/s10068-023-01303-3.
- (56) Olujimi, A. J. O. Bioactive Compounds in Ethanolic Extract of *Strychnos innocua* Root Using Gas Chromatography and Mass Spectrometry (GC-MS). *J. Community Pharm. Practice* **2021**, No. 21, 1–9.
- (57) Dias, I. A.; Horta, R. P.; Matos, M.; Helm, C. V.; Magalhães, W. L. E.; de Lima, E. A.; da Silva, B. J. G.; de Muniz, G. I. B.; de Cademartori, P. H. G. Exploring the Antioxidant and Antimicrobial Properties of the Water-Soluble Fraction Derived from Pyrolytic Lignin Separation in Fast-Pyrolysis Bio-Oil. *Biomass Convers. Biorefin.* **2023**, DOI: 10.1007/s13399-023-04561-7.
- (58) Nguyen, B. C. Q.; Shahinozaman, M.; Tien, N. T. K.; Thach, T. N.; Tawata, S. Effect of Sucrose on Antioxidant Activities and Other Health-Related Micronutrients in Gamma-Aminobutyric Acid (GABA)-Enriched Sprouting Southern Vietnam Brown Rice. *J. Cereal Sci.* **2020**, *93*, No. 102985, DOI: 10.1016/j.jcs.2020.102985.
- (59) Subramanian, S.; Dowlath, M. J. H.; Karuppanan, S. K.; Saravanan, M.; Arunachalam, K. D. Effect of Solvent on the Phytochemical Extraction and GC-MS Analysis of *Gymnema Sylvestre*. *Pharmacogn. J.* **2020**, *12* (4), 749–761.
- (60) Baldoni, L.; Marino, C. Expedient Synthesis of 1,6-Anhydro- α -D-Galactofuranose, a Useful Intermediate for Glycobiological Tools. *Beilstein J. Org. Chem.* **2014**, *10*, 1651–1656.
- (61) Gerbin, E.; Frapart, Y.-M.; Marcuello, C.; Cottyn, B.; Foulon, L.; Pernes, M.; Crônier, D.; Molinari, M.; Chabbert, B.; Ducrot, P.-H.; Baumberger, S.; Aguié-Béghin, V.; Kurek, B. Dual Antioxidant Properties and Organic Radical Stabilization in Cellulose Nanocomposite Films Functionalized by in Situ Polymerization of Coniferyl Alcohol. *Biomacromolecules* **2020**, *21*, 3163–3175, DOI: 10.1021/acs.biomac.0c00583.
- (62) Shaaban, M. T.; Ghaly, M. F.; Fahmi, S. M. Antibacterial Activities of Hexadecanoic Acid Methyl Ester and Green-Synthesized Silver Nanoparticles against Multidrug-Resistant Bacteria. *J. Basic Microbiol.* **2021**, *61* (6), 557–568.
- (63) Siswadi, S.; Saragih, G. S. *Phytochemical Analysis of Bioactive Compounds in Ethanolic Extract of Sterculia Quadrifida R.Br.* AIP Conference Proceedings; American Institute of Physics Inc., 2021.
- (64) Zheng, C. J.; Yoo, J. S.; Lee, T. G.; Cho, H. Y.; Kim, Y. H.; Kim, W. G. Fatty Acid Synthesis Is a Target for Antibacterial Activity of Unsaturated Fatty Acids. *FEBS Lett.* **2005**, *579* (23), 5157–5162.
- (65) Desbois, A. P.; Smith, V. J. Antibacterial Free Fatty Acids: Activities, Mechanisms of Action and Biotechnological Potential. *Appl. Microbiol. Biotechnol.* **2010**, *85*, 1629–1642.
- (66) Ghareeb, M. A.; Hamdi, S. A. H.; Fol, M. F.; Ibrahim, A. M. Chemical Characterization, Antibacterial, Antibiofilm, and Antioxidant Activities of the Methanolic Extract of *Paratapes Undulatus* Clams (Born, 1778). *J. Appl. Pharm. Sci.* **2022**, *12* (5), 219–228, DOI: 10.7324/JAPS.2022.120521.
- (67) Nakaziba, R.; Amana, S. B.; Sesaazi, C. D.; Byarugaba, F.; Ogwal-Okeng, J.; Alele, P. E. Antimicrobial Bioactivity and GC-MS Analysis of Different Extracts of *Corchorus Olitorius* L Leaves. *Sci. World J.* **2022**, *2022*, No. 3382302, DOI: 10.1155/2022/3382302.
- (68) He, S.; Wu, L.; Li, X.; Sun, H.; Xiong, T.; Liu, J.; Huang, C.; Xu, H.; Sun, H.; Chen, W.; Gref, R.; Zhang, J. Metal-Organic Frameworks for Advanced Drug Delivery. *Acta Pharm. Sin. B* **2021**, *2362*–2395, DOI: 10.1016/j.apsb.2021.03.019.
- (69) Simon-Yarza, T.; Giménez-Marqués, M.; Mrimi, R.; Mielcarek, A.; Gref, R.; Horcajada, P.; Serre, C.; Couvreur, P. A Smart Metal–Organic Framework Nanomaterial for Lung Targeting. *Angew. Chem., Int. Ed.* **2017**, *56* (49), 15565–15569.
- (70) Elzein Hagr, T.; Abd elmageed, M.; Eldeen Abdrazig, S. H.; Salim Holi, A.; Y Hamadnalla, H. M. GS-MS Study, Antimicrobial and Antioxidant Activity of Fixed Oil from *Ximenia Americana* L. Seeds. *Open Access J. Chem.* **2020**, *4*, 8–13.
- (71) Mazumder, K.; Nabila, A.; Aktar, A.; Farahnaky, A. Bioactive Variability and In Vitro and In Vivo Antioxidant Activity of Unprocessed and Processed Flour of Nine Cultivars of Australian Lupin Species: A Comprehensive Substantiation. *Antioxidants* **2020**, *9* (4), No. 282, DOI: 10.3390/antiox9040282.
- (72) Sheik, A.; Kim, E.; Adepelly, U.; Alhammedi, M.; Huh, Y. S. Antioxidant and Antiproliferative Activity of *Basella Alba* against Colorectal Cancer. *Saudi J. Biol. Sci.* **2023**, *30* (4), No. 103609, DOI: 10.1016/j.sjbs.2023.103609.
- (73) Swantara, M. D.; Rita, W. S.; Suartha, N.; Agustina, K. K. Anticancer Activities of Toxic Isolate of *Xestospongia Testudinaria* Sponge. *Vet World* **2019**, *12* (9), 1434–1440.
- (74) Gidik, B. Antioxidant, Antimicrobial Activities and Fatty Acid Compositions of Wild *Berberis* Spp. by Different Techniques Combined with Chemometrics (PCA and HCA). *Molecules* **2021**, *26* (24), No. 7448, DOI: 10.3390/molecules26247448.
- (75) Chandra, M.; Prakash, O.; Kumar, R.; Bachheti, R.; Bhushan, B.; Kumar, M.; Pant, A. β -Selinene-Rich Essential Oils from the Parts of *Callicarpa Macrophylla* and Their Antioxidant and Pharmacological Activities. *Medicines* **2017**, *4* (3), No. 52, DOI: 10.3390/medicines4030052.
- (76) Narra, N.; Kaki, S. S.; Prasad, R. B. N.; Misra, S.; Dhevendar, K.; Kontham, V.; Korlipara, P. V. Synthesis and Evaluation of Antioxidant and Cytotoxic Activities of Novel 10-Undecenoic Acid Methyl Ester Based Lipoconjugates of Phenolic Acids. *Beilstein J. Org. Chem.* **2017**, *13*, 26–32.
- (77) Latip, A. F. A.; Hussein, M. Z.; Stanslas, J.; Wong, C. C.; Adnan, R. Release Behavior and Toxicity Profiles towards A549 Cell Lines of Ciprofloxacin from Its Layered Zinc Hydroxide Intercalation Compound. *Chem. Cent J.* **2013**, *7* (1), No. 119, DOI: 10.1186/1752-153X-7-119.
- (78) Yousaf, A.; Zafar, A.; Ali, M.; Bukhary, S. M.; Manzoor, Y.; Tariq, T.; Saeed, A.; Akram, M.; Bukhari, F.; Abdullah, M.; Zehra, S. S.; Hassan, S. G.; Hasan, M. Intrinsic Bio-Enhancer Entities of *Fagonia Cretica* for Synthesis of Silver Nanoparticles Involves Anti-Urease, Anti-Oxidant and Anti-Tyrosinase Activity. *Adv. Biosci. Biotechnol.* **2019**, *10*, 455–468, DOI: 10.4236/abb.2019.1012032.
- (79) Zafar, A.; Jabbar, M.; Manzoor, Y.; Gulzar, H.; Hassan, S. G.; Nazir, M. A.; Mustafa, G.; Sahar, R.; Masood, A.; Iqbal, A.; Hussain, M.; Hasan, M. Quantifying Serum Derived Differential Expressed and Low Molecular Weight Protein in Breast Cancer Patients. *Protein Pept Lett.* **2020**, *27*, 658–673, DOI: 10.2174/0929866527666200110155609.
- (80) Yasmeen, M.; Momina, D.; Hassan, S. G.; Hasan, M.; Nasir, M.; Tariq, T.; Zafar, A.; Israr, S.; Tariq, F. Blueprinting in Coherence

to Diagnostic Momentum: On Account of Cancer Detection in Bahawalpur Community. *Pak. J. Biochem. Biotechnol.* **2022**, *3* (1), 64–79, DOI: 10.52700/pjbb.v3i1.107.

(81) Manzoor, Y.; Hasan, M.; Zafar, A.; Dilshad, M.; Ahmed, M. M.; Tariq, T.; Hassan, S. G.; Hassan, S. G.; Shaheen, A.; Caprioli, G.; Shu, X. Incubating Green Synthesized Iron Oxide Nanorods for Proteomics-Derived Motif Exploration: A Fusion to Deep Learning Oncogenesis. *ACS Omega* **2022**, *7*, 47996–48006, DOI: 10.1021/acsomega.2c05948.

(82) Rathore, P.; Arora, I.; Rastogi, S.; Akhtar, M.; Singh, S.; Samim, M. Collagen Nanoparticle-Mediated Brain Silymarin Delivery: An Approach for Treating Cerebral Ischemia and Reperfusion-Induced Brain Injury. *Front. Neurosci.* **2020**, *14*, No. 538404, DOI: 10.3389/fnins.2020.538404.

(83) Yousaf, A. M.; Malik, U. R.; Shahzad, Y.; Mahmood, T.; Hussain, T. Silymarin-Laden PVP-PEG Polymeric Composite for Enhanced Aqueous Solubility and Dissolution Rate: Preparation and in Vitro Characterization. *J. Pharm. Anal.* **2019**, *9* (1), 34–39.

(84) Ali, A.; Saeed, S.; Hussain, R.; Afzal, G.; Siddique, A. B.; Parveen, G.; Hasan, M.; Caprioli, G. Synthesis and Characterization of Silica, Silver-Silica, and Zinc Oxide-Silica Nanoparticles for Evaluation of Blood Biochemistry, Oxidative Stress, and Hepatotoxicity in Albino Rats. *ACS Omega* **2023**, *8* (23), 20900–20911.

(85) Ghaffar, A.; Hussain, R.; Abbas, G.; Khan, R.; Akram, K.; Latif, H.; Ali, S.; Baig, S.; Du, X.; Khan, A. Assessment of Genotoxic and Pathologic Potentials of Fipronil Insecticide in Labeo Rohita (Hamilton, 1822). *Toxin Rev.* **2021**, *40* (4), 1289–1300.

(86) Naz, I.; Khan, M. R.; Zai, J. A.; Batool, R.; Maryam, S.; Majid, M. Indigofera Linifolia Ameliorated CCl4 Induced Endoplasmic Reticulum Stress in Liver of Rat. *J. Ethnopharmacol.* **2022**, *285*, No. 114826, DOI: 10.1016/j.jep.2021.114826.

(87) Tan, T. C.; Cheng, L. H.; Bhat, R.; Rusul, G.; Easa, A. M. Composition, Physicochemical Properties and Thermal Inactivation Kinetics of Polyphenol Oxidase and Peroxidase from Coconut (Cocos Nucifera) Water Obtained from Immature, Mature and Overly-Mature Coconut. *Food Chem.* **2014**, *142*, 121–128.

(88) Marklund, S.; Marklund, G. Involvement of the Superoxide Anion Radical in the Autoxidation of Pyrogallol and a Convenient Assay for Superoxide Dismutase. *Eur. J. Biochem.* **1974**, *47* (3), 469–474.

(89) 22 FORMATION OR REMOVAL OF OXYGEN RADICALS